Electronic Supplementary Material (ESI) for Physical Chemistry Chemical Physics.

Supporting Information: Vibronic Spectroscopy of Methyl Anthranilate and its Water Complex: Hydrogen Atom Dislocation in the Excited State

Karl N. Blodgett[a], Dewei Sun[a], Joshua L. Fischer[a], Edwin L. Sibert, III[b], and Timothy S. Zwier[a]*

[a]*Department of Chemistry, Purdue University, West Lafayette, Indiana 47907-2084, United States*
[b]*Department of Chemistry, University of Wisconsin-Madison, Madison, Wisconsin 53706, United States*

Table of Contents

1. Mass-Resolved Two-Color Resonant Two-Photon Ionization Spectra (2C-R2PI) of MA and MA-H_2O

The identity of MA and MA-H_2O were confirmed with mass-resolved 2C-R2PI spectra. In this scheme, two temporally overlapped, counter-propagating UV lasers, λ_{scan} and λ_{ionize}, interact at a 90° angle with the skimmed molecular beam in the extraction region of the Time of Flight (TOF) mass-spectrometer. The ionization potential of MA and MA-H_2O are such that two photons at the absorbing 0^0_0 region (λ_{scan}) do not possess sufficient energy to ionize either species. A second, higher energy photon (λ_{ionize}) ensures that molecules that have undergone absorption of λ_{scan} are promoted to the ionization continuum. Care is taken to ensure that no ion signal is generated from either λ_{scan} or λ_{ionize} individually.

The 2C-R2PI spectra of MA and MA-H_2O are shown in **Figure S1(a)** and **S1(b)**, respectively. These spectra were recorded by monitoring ion current in the 151 and 169 amu mass channels, respectively, as a function of λ_{scan}. The same region that was recorded using LIF spectroscopy was recorded using 2C-R2PI for MA. For MA-H_2O, only the first ~250 cm^{-1} region was recorded. The peak positions, in both cases, verify the identity of the species.

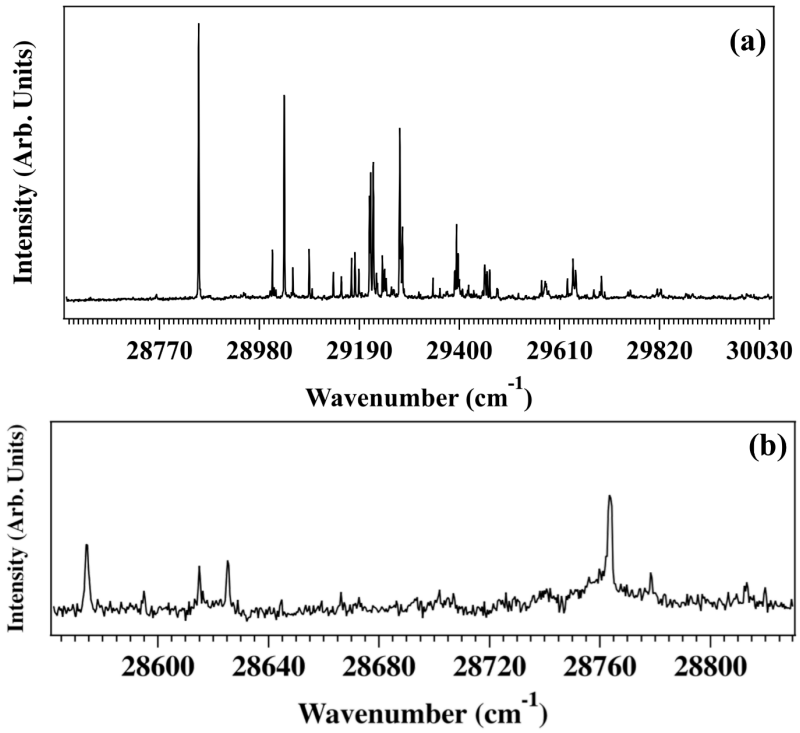

Figure S1: 2C-R2PI spectra of MA (a) and MA-H_2O (b).

2. Rotamers of MA

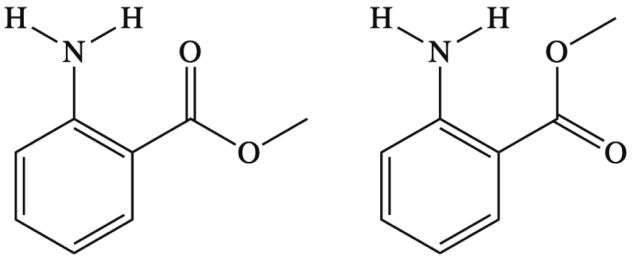

0.0 kJ/mol **13.3 kJ/mol**

Figure S2: The two low-energy rotamers of MA. Zero-point corrected energies calculated at the DFT B3LYP-D3BJ/def2TZVP level of theory.

3. NH_2 Inversion Potential of MA

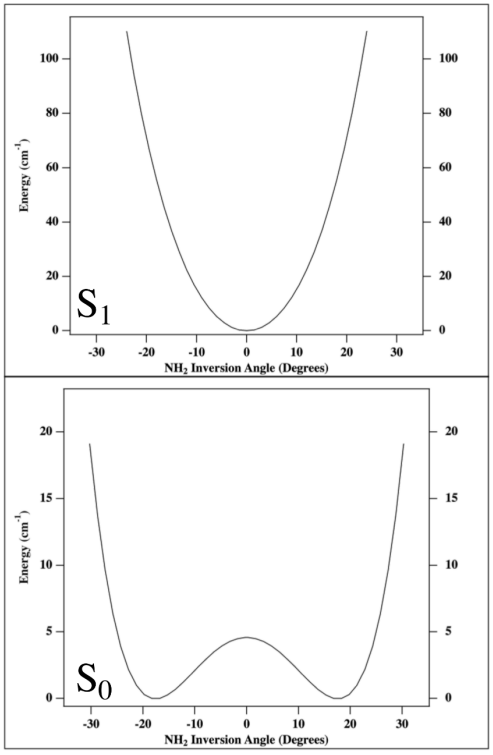

Figure S3: Relaxed potential energy scans about the improper CNHH dihedral defining the NH_2 inversion in MA, in the S_0 (bottom) and S_1 (top) electronic states.

4. Molecular Orbitals Involved in Electronic Transitions of MA

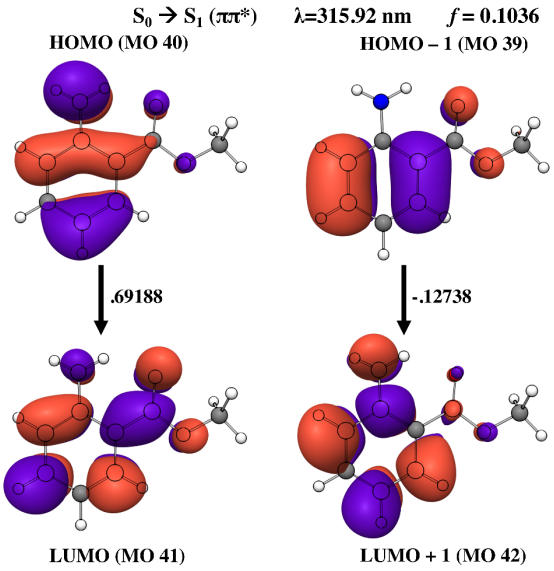

Figure S4: Molecular orbitals involved in the S_0 - S_1 electronic transition of MA, along with the coefficients, calculated vertical excitation wavelength, and oscillator strength. Calculations performed at the DFT B3LYP-D3BJ/def2TZVP level of theory

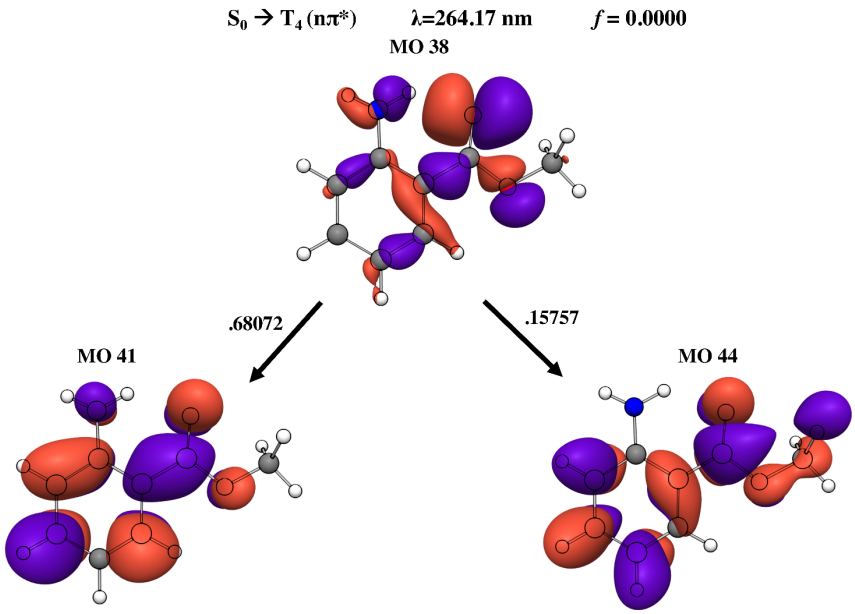

Figure S5: Molecular orbitals involved in the S_0 - T_4 electronic transition of MA, along with the coefficients, calculated vertical excitation wavelength, and oscillator strength. Calculations performed at the DFT B3LYP-D3BJ/def2TZVP level of theory.

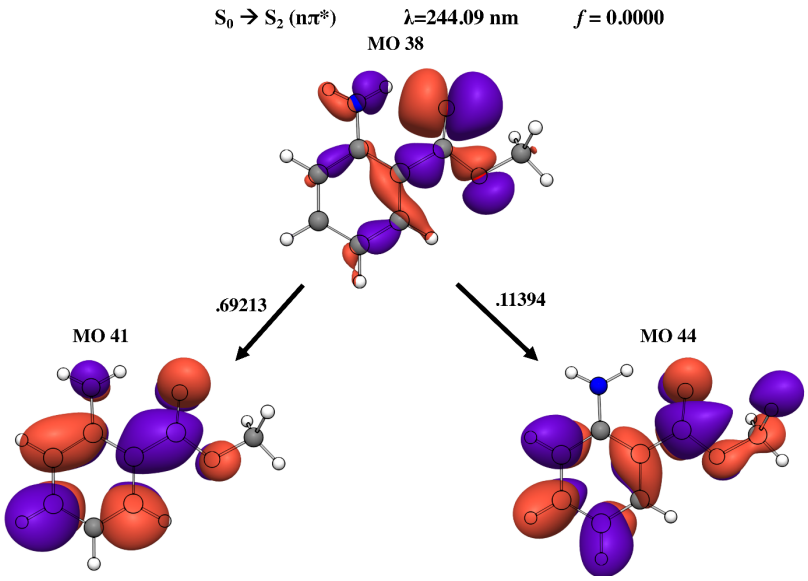

Figure S6: Molecular orbitals involved in the S_0 - S_2 electronic transition of MA, along with the coefficients, calculated vertical excitation wavelength, and oscillator strength. Calculations performed at the DFT B3LYP-D3BJ/def2TZVP level of theory.

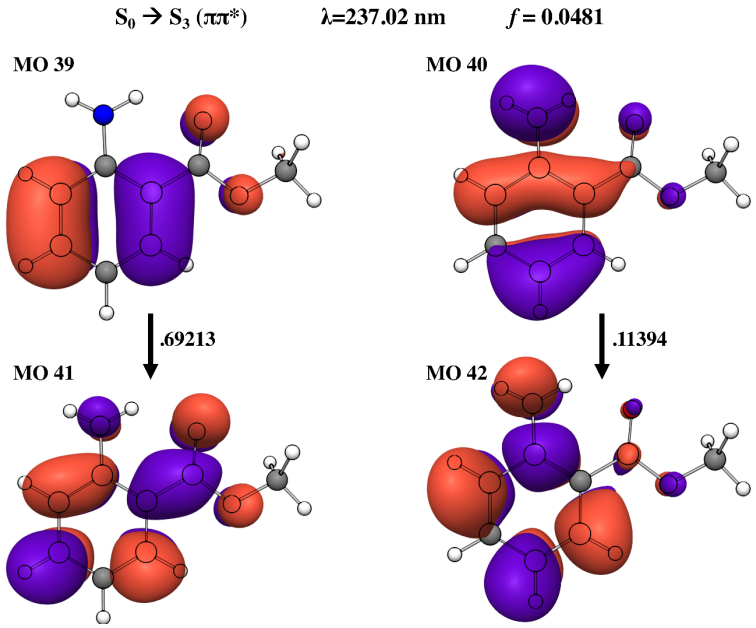

Figure S7: Molecular orbitals involved in the S_0 - S_3 electronic transition of MA, along with the coefficients, calculated vertical excitation wavelength, and oscillator strength. Calculations performed at the DFT B3LYP-D3BJ/def2TZVP level of theory.

5. Fluorescence Decay Traces of MA and MA-H_2O

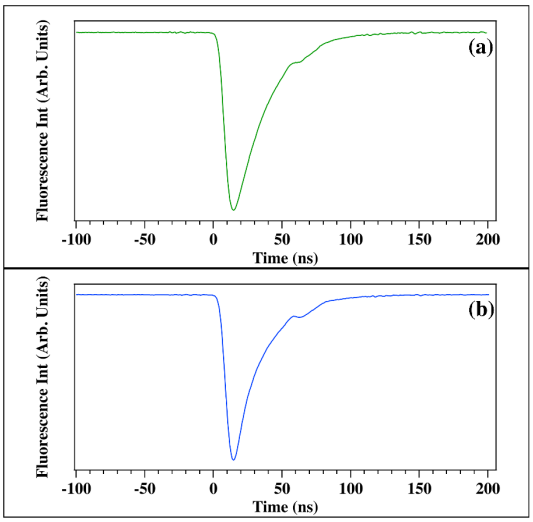

Figure S8: Fluorescence decay traces of (a) MA and (b) MA-H_2O. Lifetimes were obtained by fitting each trace to a single exponential decay and extracting the time constant, τ (lifetime). The lifetime is measured to be 27 ns for MA and 23 ns for MA-H_2O.

6. Rotational Band Contour of the Electronic Origin of MA

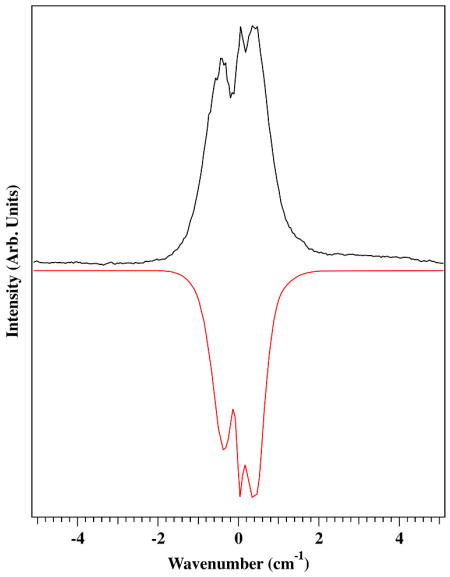

Figure S9: Rotational band contour (RBC) scan of the electronic origin transition (top trace), taken at a UV laser resolution of 0.15 cm^{-1}. The bottom trace is the computed fit using the calculated transition dipole moment (*a:b:c* = 77:23:0) components and rotational constants from calculated ground and excited states. This fit was computed using the JB95 spectral fitting program.[1]

7. Dispersed Fluorescence Spectra of Vibronic Bands with Increasing Energy in MA

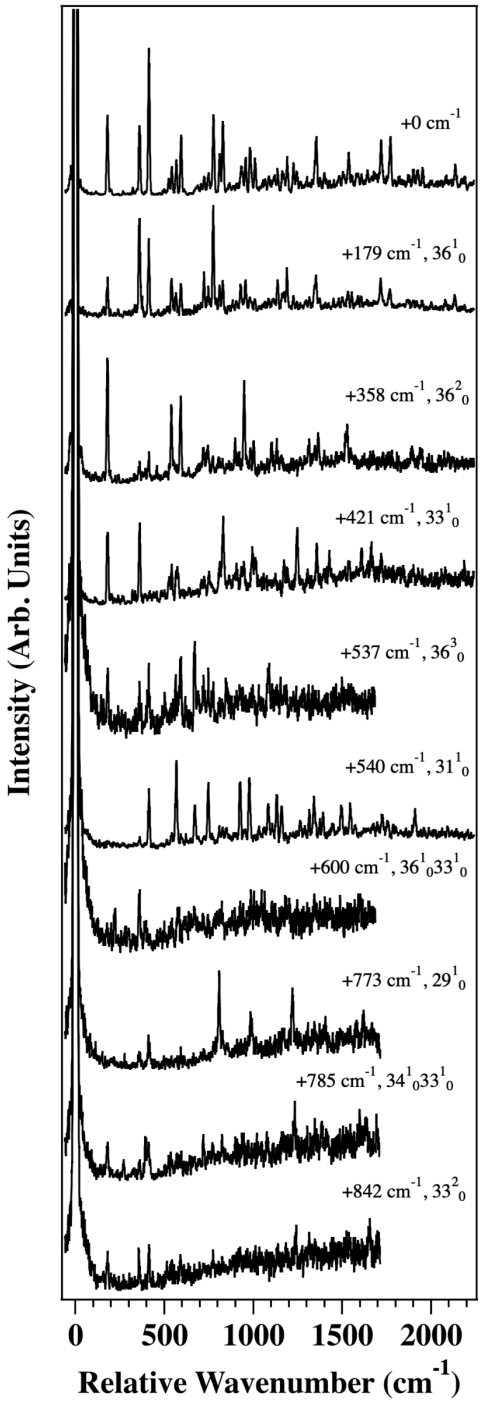

Figure S10: DFL spectra taken at increasing energies from the origin transition in MA.

8. Fermi Resonance Analysis

As described in the main text, two pairs of peaks in the LIF spectrum were identified as Fermi-Resonance pairs (see **Figure S11**). These pairs are assigned to the $50^1_0 52^1_0$ combination and Franck-Condon allowed 35^1_0 fundamental transition, and the $50^1_0 51^1_0$ combination and Franck-Condon allowed 34^1_0 fundamental transition. The DFL spectra collected from each member of the second pair of Fermi-mixed transitions is shown in **Figure S12**. The $\Delta v=0$ emission to both the $50_1 51_1$ and 34_1 ground state levels enables a quantitative analysis of the Fermi resonance mixing coefficients, α and β, to which we now turn.

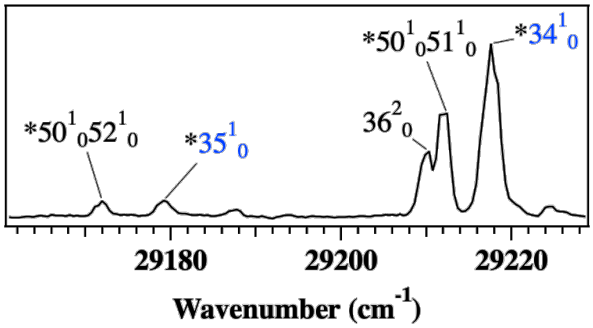

Figure S11: The portion of the LIF spectrum containing the two pairs of Fermi-mixed vibronic levels, marked with asterisks.

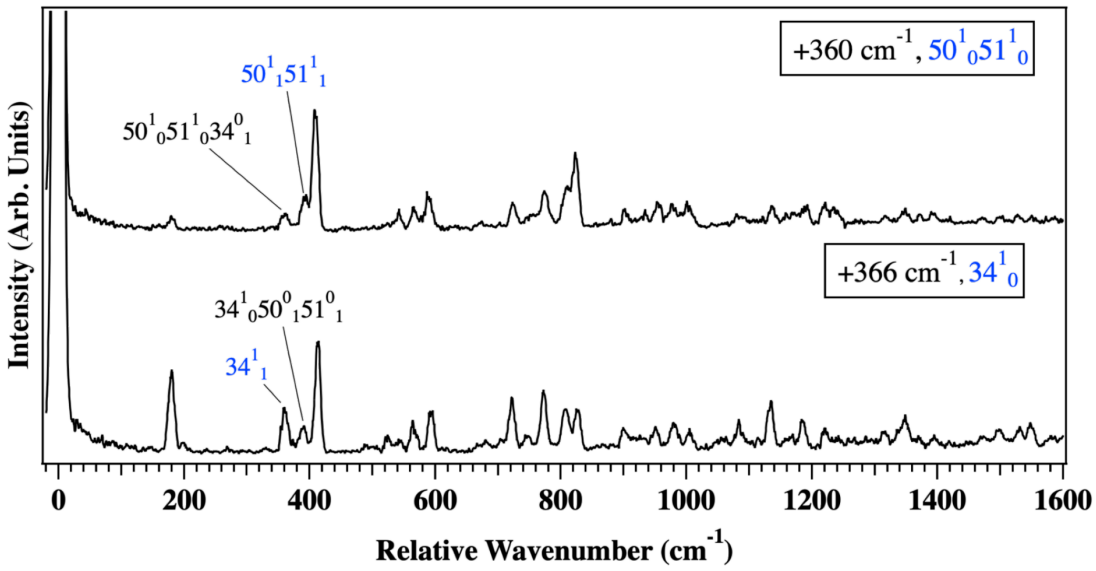

Figure S12: DFL spectra collected from each member of the Fermi-mixed $50^1_0 51^1_0$ combination and Franck-Condon allowed 34^1_0 fundamental transitions.

In the S_1 electronic state, the Fermi-mixed wavefunctions may be expressed, using bra-ket notation, as a linear combination of the unmixed wavefunctions,

$$|\psi_{366}\rangle = \alpha|a'\rangle + \beta|2a''\rangle$$

$$|\psi_{360}\rangle = \beta|a'\rangle - \alpha|2a''\rangle$$

Where $|a'\rangle$ is the S_1 34^1 wavefunction, $|2a''\rangle$ is the S_1 50^151^1 wavefunction, α and β are the mixing coefficients. Solving for the Franck-Condon factor (FCF) from the S_0 zero-point level, $\langle 0|$, to each of these S_1 vibrational levels, and assuming that the wavefunction overlap $\langle 0|2a''\rangle$ is negligible, we obtain

$$\mathbf{FCF_{0,366}} = |\langle 0|\psi_{366}\rangle|^2 = \alpha^2|\langle 0|a'\rangle|^2$$

and

$$\mathbf{FCF_{0,360}} = |\langle 0|\psi_{360}\rangle|^2 = \beta^2|\langle 0|a'\rangle|^2$$

Taking the ratio

$$\mathbf{FCF_{0,366}}/\ \mathbf{FCF_{0,360}} = \alpha^2/\beta^2$$

gives the relative intensities of the vibronic bands in the LIF spectrum. Integrating these experimental bands, we obtain

$$\alpha^2/\beta^2 = 1.80$$

Solving the FCF integrals for the projection of each Fermi-mixed S_1 level onto the individual S_0 components, $\langle a'|$ (34_1) and $\langle a''|$ (50_151_1), we obtain

$$|\langle a'|\psi_{366}\rangle|^2/|\langle 2a''|\psi_{366}\rangle|^2 = (\alpha^2|\langle a'|a'\rangle|^2)/(\beta^2|\langle 2a''|2a''\rangle|^2) = \alpha^2/\beta^2 = 1.80$$

and

$$|\langle a'|\psi_{360}\rangle|^2/|\langle 2a''|\psi_{360}\rangle|^2 = (\beta^2|\langle a'|a'\rangle|^2)/(\alpha^2|\langle 2a''|2a''\rangle|^2) = \beta^2/\alpha^2 = 0.55$$

where we have assumed a 1:1 correspondence between analogous S_0 and S_1 normal modes (i.e., no Duschinsky mixing). From the experimental DFL spectra, we measure the relative integrated intensities to be

$$|\langle a'|\psi_{366}\rangle|^2/|\langle 2a''|\psi_{366}\rangle|^2 = 1.70$$

and

$$|\langle a'|\psi_{360}\rangle|^2/|\langle 2a''|\psi_{360}\rangle|^2 = 0.52$$

The good agreement between calculated and measured peak intensities allows us to express the normalized S_1 Fermi-mixed wavefunctions as

$$|\psi_{366}\rangle = 0.802|a'\rangle + 0.597|2a''\rangle$$

$$|\psi_{360}\rangle = 0.597|a'\rangle - 0.802|2a''\rangle$$

As anticipated, the excited state level +366 cm^{-1} above the S_1 ZPL is about 64% 34^1 and 36% 50^151^1, while the one at 360 cm^{-1} is the reverse; that is, 36% 34^1 and 64% 50^151^1 (see **Figure S11**).

9. Low-Energy Water Complex Conformers

In addition to the assigned MA-H_2O water complex, several other low-energy conformational minima were found. These conformers, along with their basis-set superposition error (BSSE) corrected and/or zero-point (ZPE) corrected energies are presented in **Table S1** and **Figure S13**.

Table S1: Relative zero-point corrected potential energies, BSSE and zero-point corrected potential energies, adiabatic and vertical excitation energies of the water complex conformers calculated to lie within 10 kJ/mol of the global minimum. Calculations performed at the DFT B3LYP-D3BJ/def2TZVP level of theory.

Complex	ZPE corr. Electronic energy (kJ/mol)	BSSE and ZPE corr. Electronic energy (kJ/mol)	TD-DFT Adiabatic S_0-S_1 Excitation Energy (cm^{-1})	TD-DFT Vertical S_0-S_1 Excitation Energy (cm^{-1})
MAw3 (assigned)	0	0	27,095	31,020
MAw4	0.299307	1.79729889	27,004	30,973
MAw8	3.7518395	3.243491765	27,171	30,928
MAw2	3.0482055	4.109389542	26,606	32,247
MAw1	4.6865175	5.209882307	27,534	32,923
MAw12	5.30351	5.344971633	27,345	31,299
MAw9	4.6812665	5.352848133	27,220	32,995

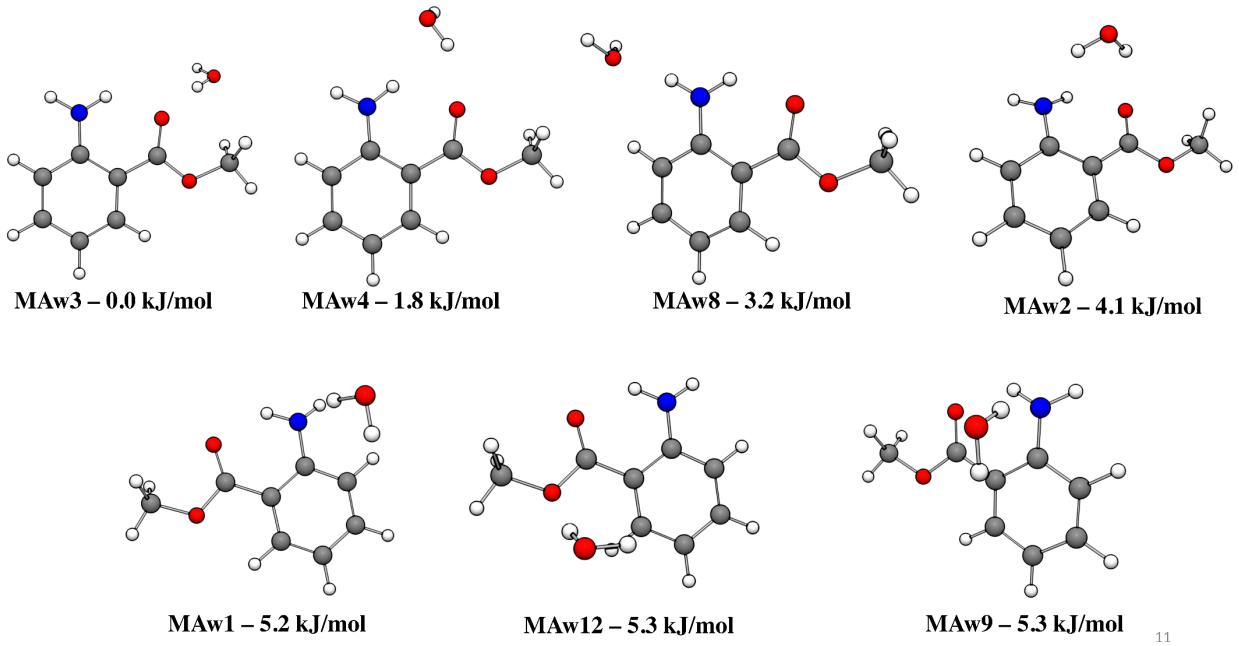

Figure S13: All MA-H_2O conformers, with their BSSE/ZPE-corrected energies, calculated to lie within 10 kJ/mol of the global minimum.

10. Molecular Orbitals Involved in Electronic Transitions of MA-H_2O

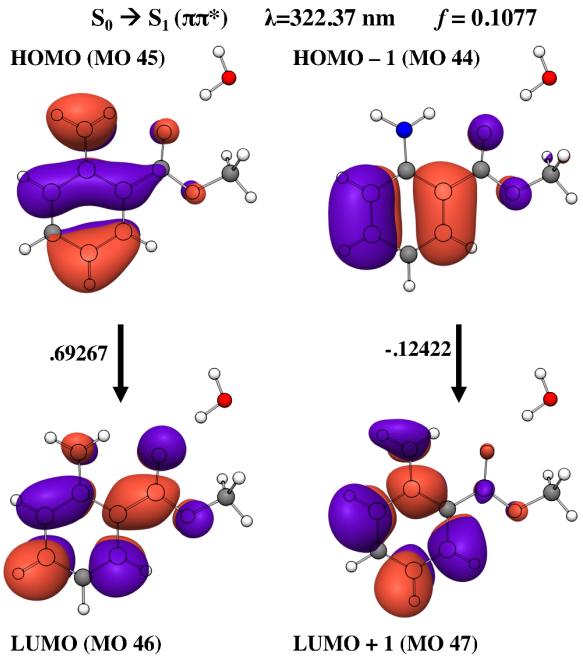

Figure S14: Molecular orbitals involved in the S_0 - S_1 electronic transition of MA-H_2O, along with the coefficients, calculated vertical excitation wavelength, and oscillator strength. Calculations performed at the DFT B3LYP-D3BJ/def2TZVP level of theory.

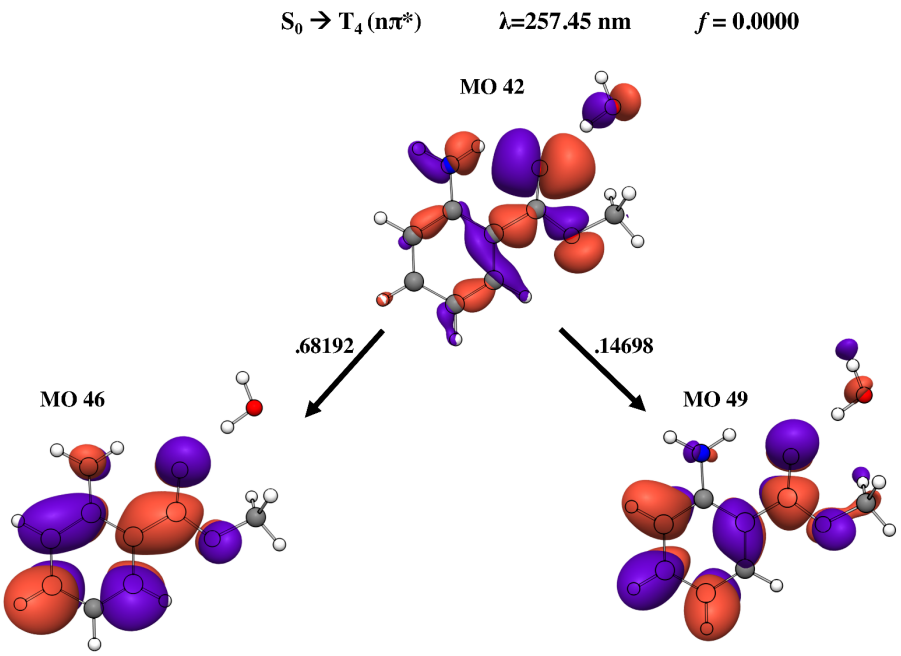

Figure S15: Molecular orbitals involved in the S_0 - T_4 electronic transition of MA-H_2O, along with the coefficients, calculated vertical excitation wavelength, and oscillator strength. Calculations performed at the DFT B3LYP-D3BJ/def2TZVP level of theory.

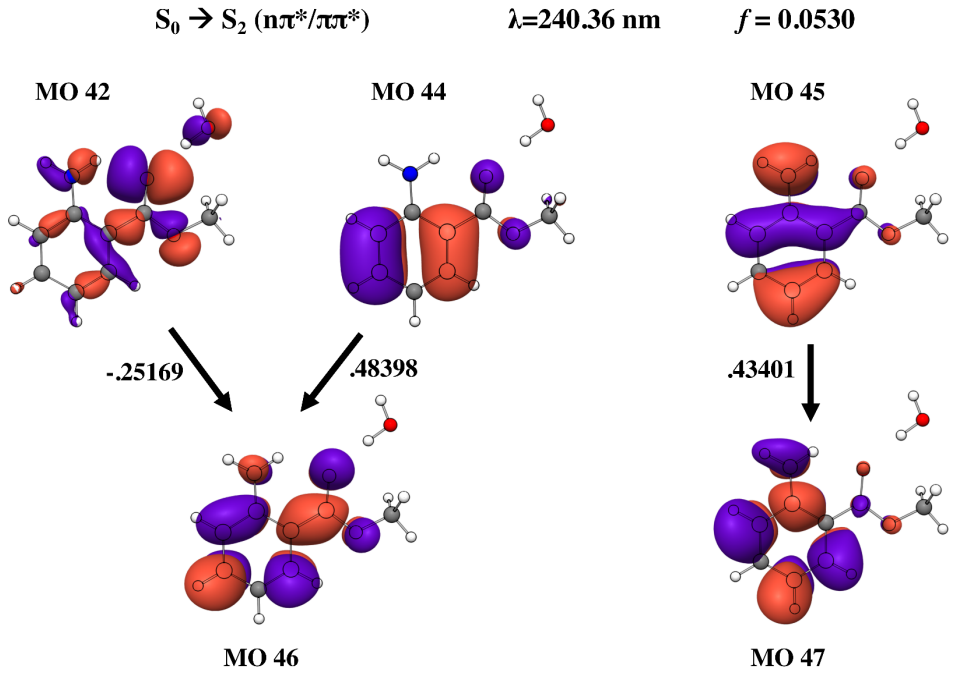

Figure S16: Molecular orbitals involved in the S_0 - S_2 electronic transition of MA-H_2O, along with the coefficients, calculated vertical excitation wavelength, and oscillator strength. Calculations performed at the DFT B3LYP-D3BJ/def2TZVP level of theory.

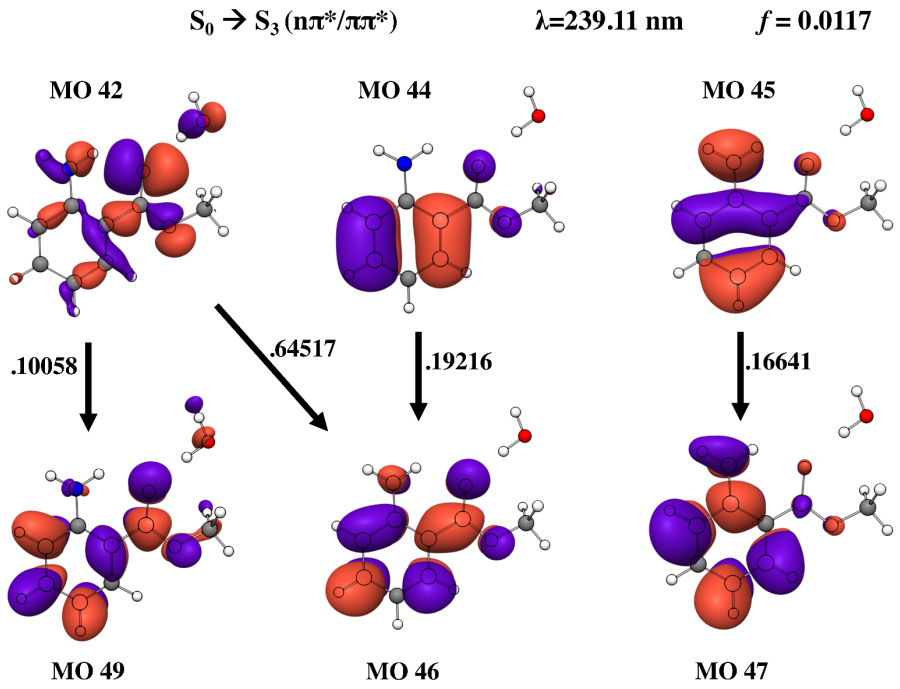

Figure S17: Molecular orbitals involved in the S_0 - S_3 electronic transition of MA-H_2O, along with the coefficients, calculated vertical excitation wavelength, and oscillator strength. Calculations performed at the DFT B3LYP-D3BJ/def2TZVP level of theory.

11. Normal Modes, and Reduced Duschinsky Matrix, of MA-H_2O

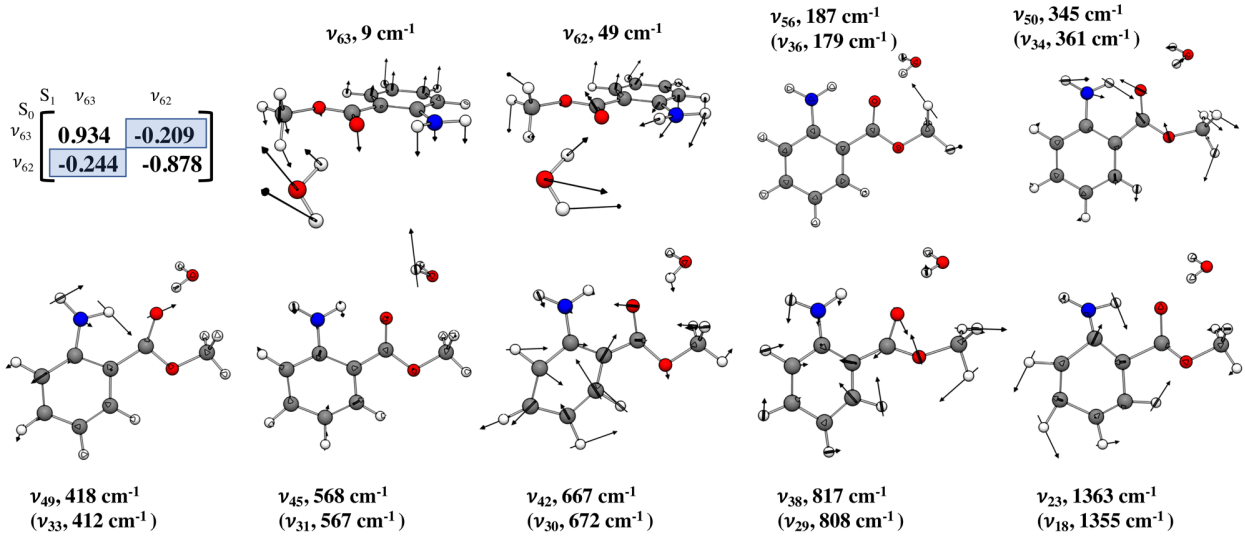

Figure S18: Reduced Duschinsky rotation matrix, and vector displacement representation of the Franck-Condon active normal modes of MA-H_2O. Values in parentheses are those corresponding values in the MA monomer. Calculations performed at the DFT B3LYP-D3BJ/def2TZVP level of theory.

12. Aniline S_0 and S_1 Calculated Geometries and Molecular Orbital Transitions

$S_0 \rightarrow S_1$ ($\pi\pi^*$) λ=261.30 nm f = 0.0359

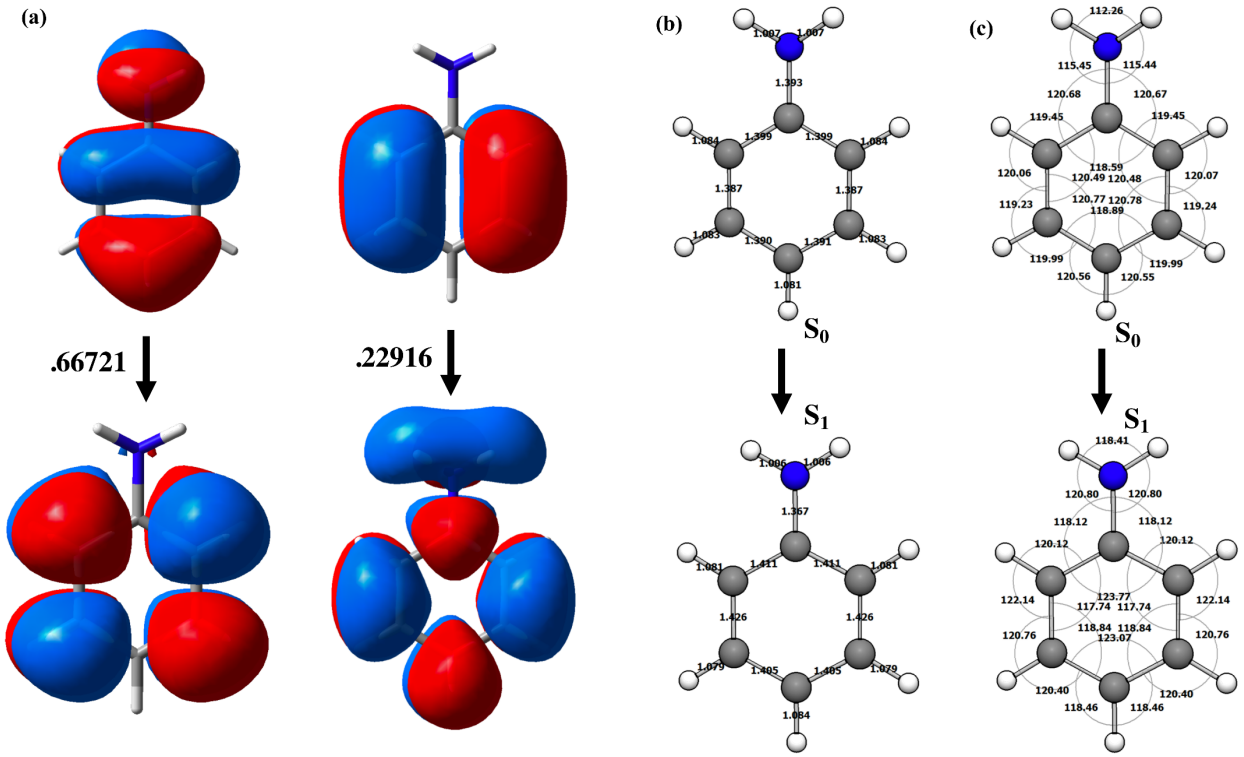

Figure S19: The (a) molecular orbitals, transition coefficients, oscillator strength, (b) bond distance, and (c) bond angle parameters associated with the S_0 - S_1 transition of aniline. Calculations performed at the DFT B3LYP-D3BJ/def2TZVP level of theory.

13. Methyl Benzoate S_0 and S_1 Calculated Geometries and Molecular Orbital Transitions

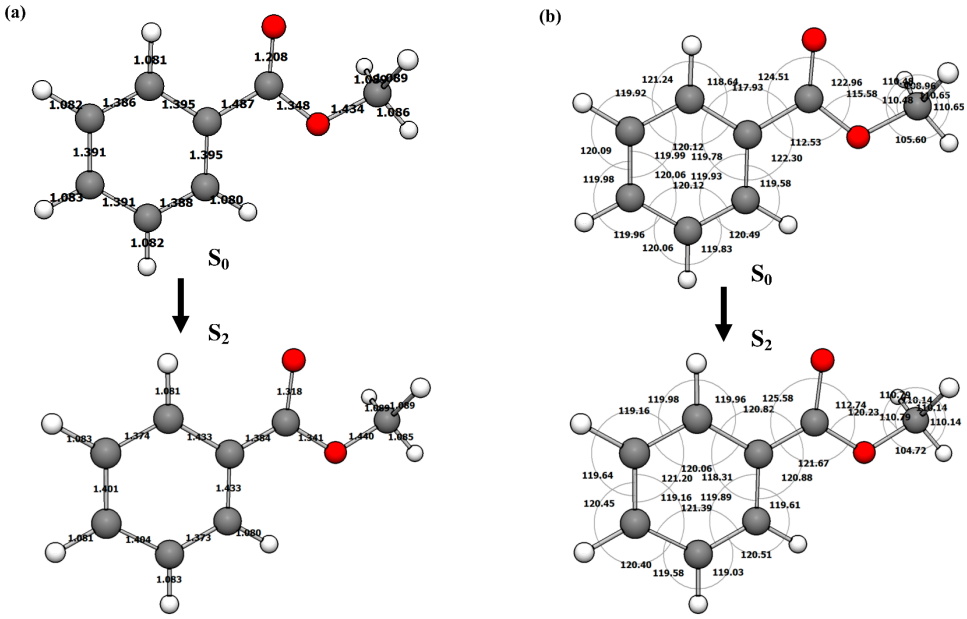

Figure S20: The (a) bond distance, and (b) bond angle parameters associated with the S_0 - S_2 transition of methyl benzoate. Calculations performed at the DFT B3LYP-D3BJ/def2TZVP level of theory.

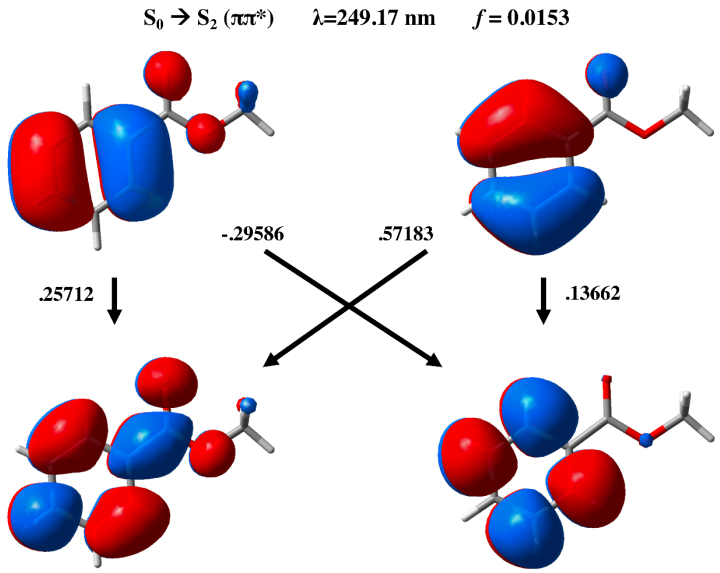

Figure S21: Molecular orbitals involved in the S_0 - S_2 electronic transition of methyl benzoate, along with the coefficients, calculated vertical excitation wavelength, and oscillator strength. Calculations performed at the DFT B3LYP-D3BJ/def2TZVP level of theory.

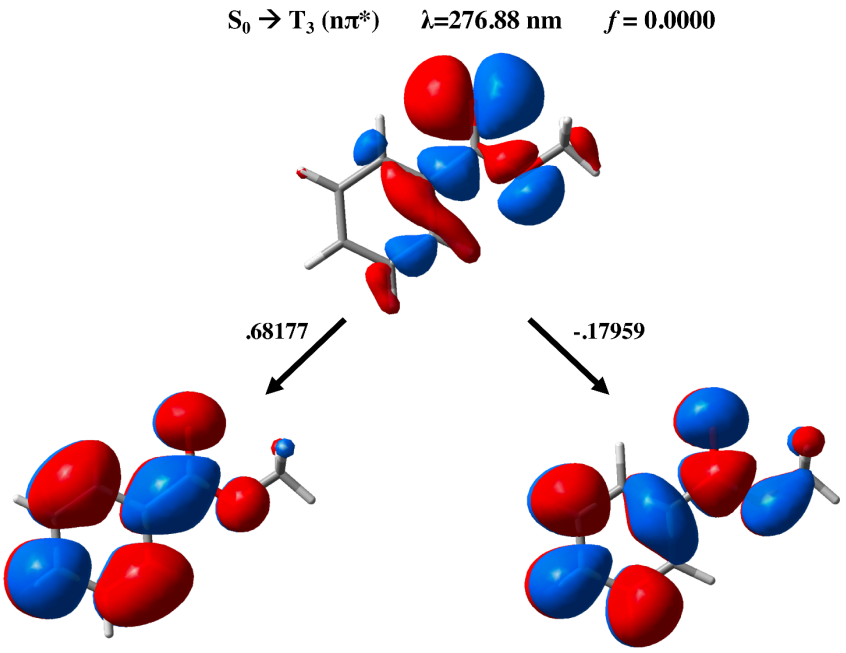

Figure S22: Molecular orbitals involved in the S_0 - T_3 electronic transition of methyl benzoate, along with the coefficients, calculated vertical excitation wavelength, and oscillator strength. Calculations performed at the DFT B3LYP-D3BJ/def2TZVP level of theory.

14. Comparison of the Anthranilates

The results presented herein allow us to compare similar systems to one another. We begin with MA and MA-H_2O. As we saw in section III, the LIF excitation and 0^0_0 DFL spectra of MA and MA-H_2O are quite similar to one another, with analogous modes dominating the spectra of both. Aside from breaking the C_s symmetry of the monomer unit, the effect of water binding on molecular structure, and therefore, vibrational frequencies, seems to have little effect. This is evident by the small shift in analogous Franck-Condon active frequencies between hydrated and non-hydrated MA, shown in **Table 2** of the main text. The MA-H_2O 0^0_0 transition is 278 cm^{-1} lower energy than that of MA. In a simple estimation, this shift may be explained by the polarization of molecular orbitals involved in the electronic transition by the water interaction.

The structural changes that occur in MA upon UV excitation also occur in MA-H_2O, to a degree that is modulated by the water interaction. Upon excitation in MA-H_2O the aromatic ring flattens, the amine group tilts toward the methoxycarbonyl group, closing the C6 ring formed by

the NH···O=C hydrogen bond. The N-H_{donor} bond increases in length by 0.022 Å, the O=C bond increases in length by 0.034 Å, resulting in a decrease of the H···O hydrogen bonding distance by 0.180 Å (going from 1.935 to 1.755 Å). **Table 3** in the main text lists the S_0, S_1, and difference in structural parameters for MA and MA-H_2O. The water molecule rotates and moves out of plane (see **Figure 11** in the main text). This has the effect of decreasing the OH···O=C hydrogen bonding distance by 0.080 Å and increasing the H_2O···CH_3 distance by 0.220 Å. We see, then, that the structural change of MA-H_2O upon electronic excitation proceeds along the same hydrogen dislocation coordinate as that of MA, to a degree determined by the H_2O interaction.

Time dependent density functional theory results indicate that the electronic S_0-S_1 transition in both MA and MA-H_2O may be described by two single-electron transitions from one molecular orbital to another. The molecular orbitals responsible for these transitions in MA and MA-H_2O are shown in **Figure S4** and **S14**. The orbitals, and coefficients, involved in the electronic transition in each case are nearly identical to one another and may be described as a textbook example of conjugated π bonding orbitals moving electron density onto conjugated π* anti-bonding orbitals.

The nature of the structural change upon electronic excitation between MA and AA are very similar to one another. Hydrogen atom dislocation occurs in each case.[2] The LIF excitation spectrum of each species also has progressions in the same normal modes, designated as modes ν_{36} and ν_{33} in MA. The single water complexes of MA and AA are also quite similar to one another.[3] In each case, a water hydrogen bonds with the monomer C=O. In AA-H_2O, an additional hydrogen bond is formed between the water oxygen and monomer acid H-O group, which MA lacks. The absence of water hydrogen bonding with the NH_2 in each case is perhaps not surprising, given the extremely strong hydrogen bond in which the amine group is already participating.

15. Franck-Condon Analysis

To further quantify the difference between excited and ground electronic states of MA, we carried out one-dimensional Franck-Condon analyses of nearly all vibronically active normal modes. Harmonic Franck-Condon overlap integrals were calculated as a function of the parameters *D* and δ, which represent normal coordinate displacement upon excitation and square root of the ratio between ground and excited state vibrational frequencies, respectively[4]. *D* is varied to find the best fit between calculated and experimental excitation and DFL spectra of the members of the progression under consideration. **Figures S23** and **S24** show the calculated fits to the members of the 421 and 179 cm^{-1} progressions, respectively. The best fit displacement value for these modes is 1.27 and 0.97, respectively. We find that, while the over-all fits are reasonably good, the spectral fits do not quantitatively emulate the DFL and LIF excitation spectra simultaneously, in that the best fits to the series of DFL spectra require larger Franck-Condon activity in excitation than is observed experimentally. Since the UV-D spectra shows no non-radiative turn on over the wavelength region we are probing, this is an indication that a one-dimensional analysis is not sufficient for the vibronic spectra of MA, which is further evidence of Duschinsky mixing in MA between the ground and excited state normal coordinates.

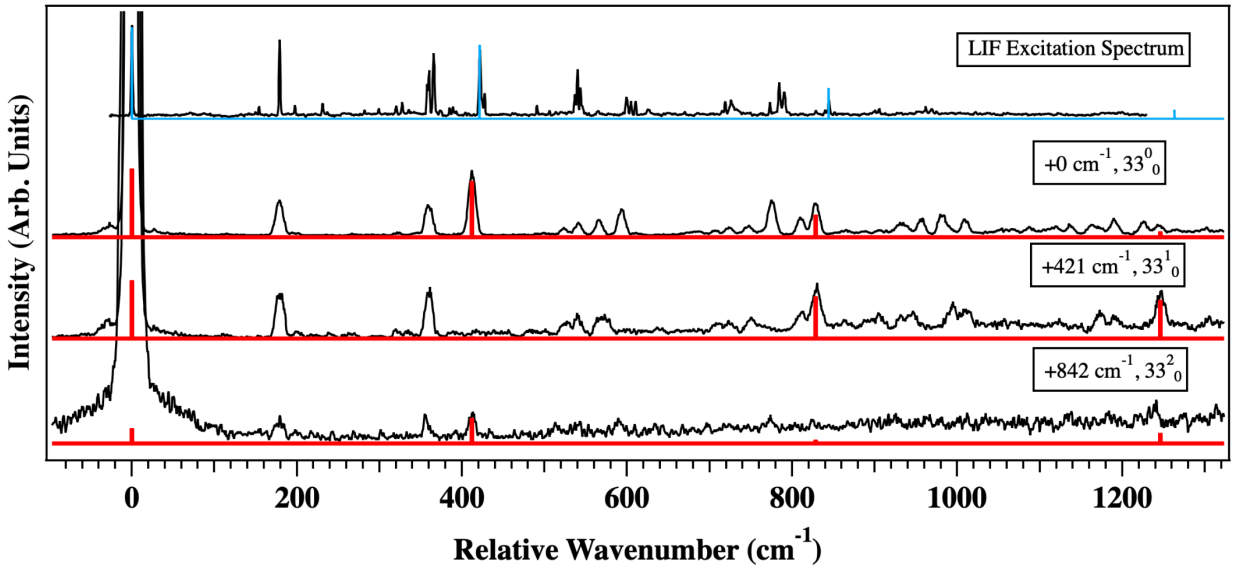

Figure S23: Franck-Condon factor fits of the members of the mode 33 progression. The best fit displacement for this mode is 1.27

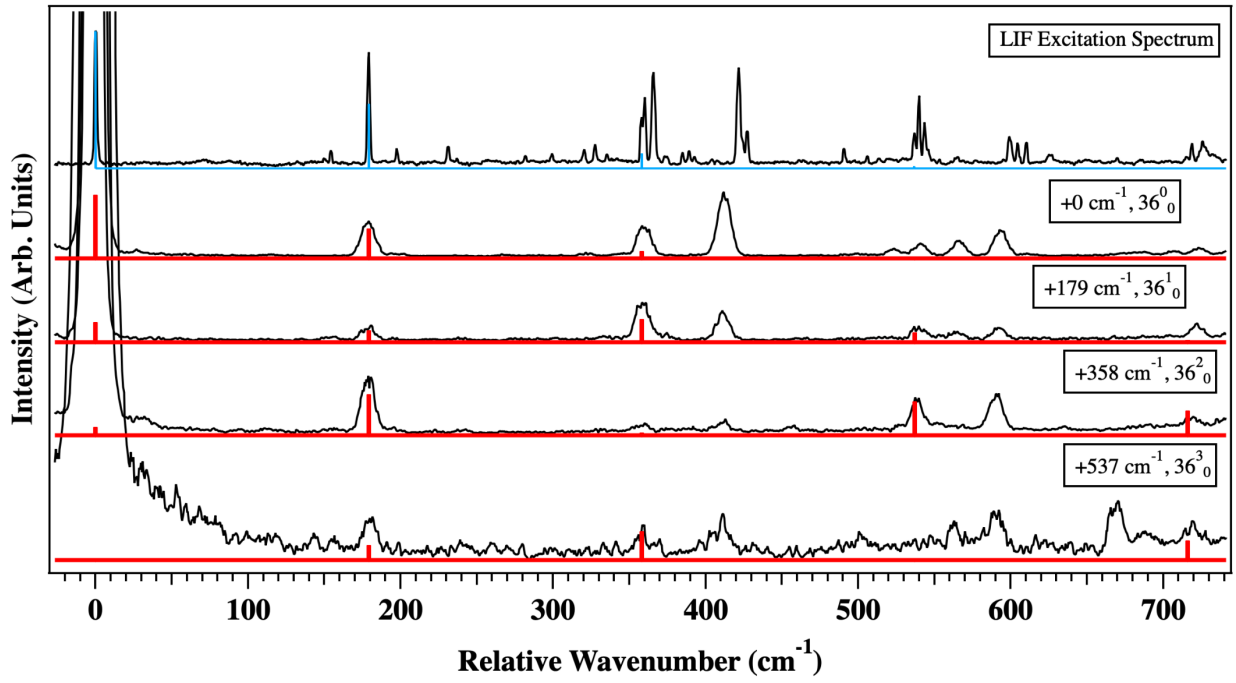

Figure S24: Franck-Condon factor fits of the members of the mode 36 progression. The best fit displacement for this mode is 0.97.

16. Transition Dipole Moment Vectors of Methyl Anthranilate, Aniline, and Methyl Benzoate

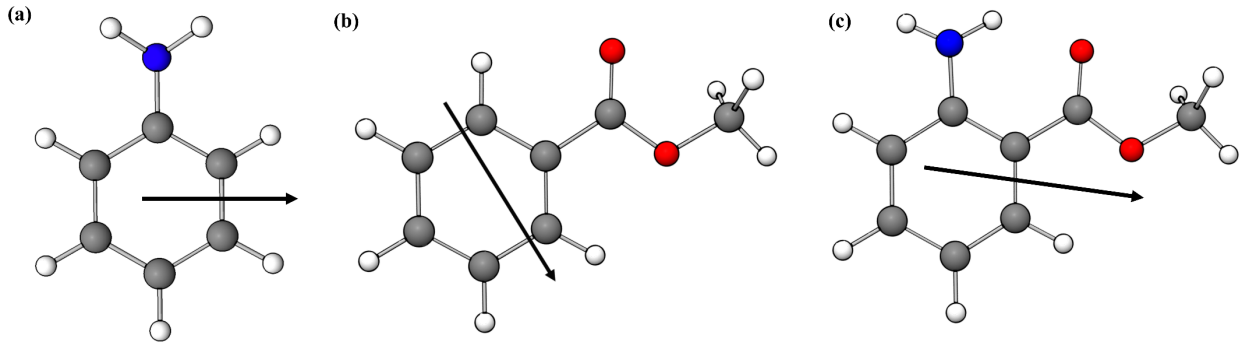

Figure S25: Transition dipole moment vectors for the lowest energy 'bright' S_0 - S_n electronic transition of (a) aniline (S_0 - S_1), (b) methyl benzoate (S_0 - S_2), and (c) methyl anthranilate (S_0 - S_1).

References

1. D. F. Plusquellic, R. Suenram, B. Mate, J. Jensen and A. Samuels, *J. Chem. Phys.*, 2001, **115**, 3057-3067.
2. C. A. Southern, D. H. Levy, G. M. Florio, A. Longarte and T. S. Zwier, *J. Phys. Chem. A*, 2003, **107**, 4032-4040.
3. J. A. Stearns, A. Das and T. S. Zwier, *PCCP*, 2004, **6**, 2605-2610.
4. J. R. Henderson, M. Muramoto and R. A. Willett, *J. Chem. Phys.*, 1964, **41**, 580-581.